Scripta Materialia 177 (2020) 96–100

Contents lists available at ScienceDirect

Scripta Materialia

journal homepage: www.elsevier.com/locate/scriptamat

Formation of refined grains below 10 nm in size and nanoscale interlocking in the particle–particle interfacial regions of cold sprayed pure aluminum

Zhiying Liu[a,1], Hongze Wang[a,1], Michel Haché[a], Eric Irissou[b], Yu Zou[a,*]

[a] Department of Materials Science and Engineering, University of Toronto, Toronto, ON M5S 3E4, Canada
[b] National Research Council Canada (NRC), Boucherville, QC J4B 6Y4, Canada

ARTICLE INFO

Article history:
Received 20 July 2019
Revised 31 August 2019
Accepted 15 September 2019
Available online 21 October 2019

Keywords:
Plastic deformation
Recrystallization
Nanostructures
Cold spray
Pure aluminum

ABSTRACT

It has been a long-standing challenge to obtain nanocrystalline pure aluminum with grain sizes below 10 nm by plastic deformation. Here, we studied the microstructure characteristics of two bonded pure aluminum powder particles after a cold spray process. In the particle–particle bonding region, nanometer-sized grains are revealed, about 30% of which are below 10 nm in size. In the particle–particle interface, we observe nanoscale perturbations with interlocking features assisting mechanical bonding. The formation of nanoscale grains and interlocking features is attributed to the extremely high strain and strain rate combined with shear instability in the cold spray process.

When the grain size of metals is reduced to about 10–100 nm, many interesting and useful properties emerge in such nanocrystalline materials, especially for high strength applications [1–3]. Grain refinement towards the nanometer-sized regime has been highly desirable for both scientific curiosity and technical applications. Over the past three decades, several methods have been used to obtain nanoscale grains, including ball milling [4], high-pressure torsion (HPT) [5], equal channel angular pressing (ECAP) [6], accumulative roll bonding (ARB) [7], and surface mechanical grinding treatment (SMGT) [8]. For metals with low or medium stacking fault energies (SFEs) (e.g., copper, nickel, and many alloys), there have been many studies that reported grain refinement below 100 nm and even below 10 nm [3,9]. However, the formation of nanoscale grains for metals with high SFEs and low melting temperatures, such as pure aluminum, is rather difficult, because their low activation energies for dislocation annihilation facilitate the recovery process which leads to insufficient dislocation density for dislocation-assisted grain refinement [10]. In literature, it has been rarely reported that pure aluminum exhibits nanoscale (<100 nm) microstructure. Very recently, Xu et al. [11] summarized the average grain/structure sizes of pure aluminum achieved using different methods: ~250 nm in cold rolling (CR) [5,12], ~600 nm in ECAP [6], ~1200 nm in HPT [5], and ~450 nm in ARB [7]. Although grain sizes in the range of 10–50 nm have been obtained using the magnetron co-sputtering technique [13], the minimum grain size induced by plastic deformation in pure aluminum is in the range of 48–68 nm, which was achieved by long hour ball milling [4] and SMGT at liquid nitrogen temperature [11]. In these cases, the formation of ultrafine grains is attributed to the high strain (up to 12), high strain rate (up to 10^3 s^{-1}), and low temperature (77 K) conditions [11]. However, the formation of grain sizes < 10 nm by plastic deformation in pure aluminum has been scarcely reported.

Cold spray (CS), as a solid-state additive manufacturing (AM) technology, produces thick coatings and bulk components through the high-velocity (500–1200 m/s) impact of solid powder particles (1–50 μm) [14]. Due to their low density, good ductility, and excellent corrosion resistance, aluminum and its alloys have been widely used to produce cold spray coatings [15]. In the CS process, such high-speed impact leads to ultrahigh strain (up to 12), strain rate (up to 10^9 s^{-1}), and cooling rate (up to 10^{10} K/s), which play essential roles in grain refinement in the particle–particle bonding regions [16,17]. Although nanocrystalline structures on the order of 20 nm have been observed in cold-sprayed aluminum alloys such as Al 5083 [18], the microstructure of cold sprayed *pure* aluminum is much less reported. While fine grains (~50–100 nm in size) have been reported in cold sprayed pure aluminum [19,20], the grain size distribution in particle–particle bonding regions, which

* Corresponding author.
E-mail address: mse.zou@utoronto.ca (Y. Zou).
[1] Contributed equally.

https://doi.org/10.1016/j.scriptamat.2019.09.018
1359-6462/

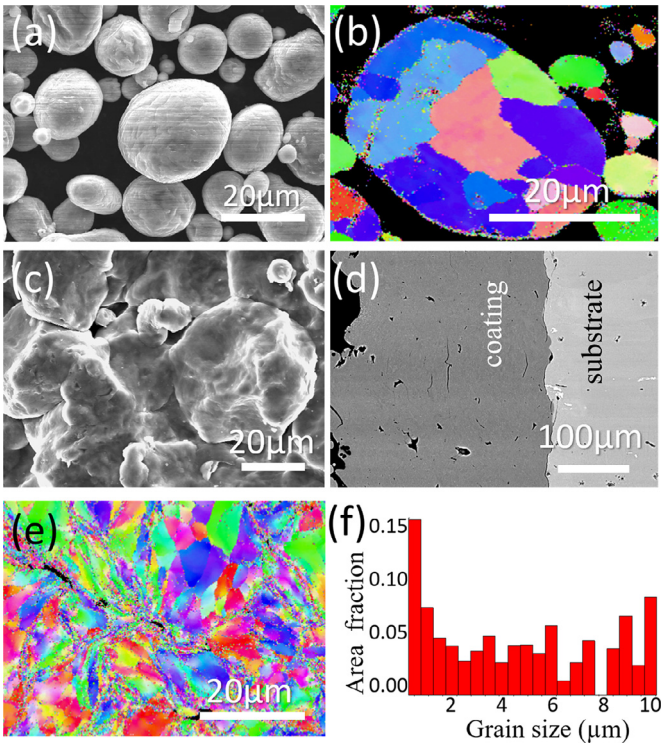

Fig. 1. (a) SEM micrograph and (b) EBSD orientation map of as-received aluminum powder particles. In the EBSD map, each point is colored according to crystal orientation, red corresponds to the [001] direction, blue to [111] and green to [101]; SEM micrographs of (c) the top surface and (d) the cross-section of as-sprayed coating; (e) EBSD map of the cross-section of as-sprayed coating and (f) its corresponding grain size distribution. (For interpretation of the references to color in this figure legend, the reader is referred to the web version of this article.)

experiences the most extreme deformation conditions, is still not very clear.

In addition, there is an ongoing debate about the bonding mechanism in cold spray coatings, between adiabatic shear instability [21–23] and hydrodynamic plasticity due to strong pressure waves [24]. Coupling of the bonding and grain refinement mechanisms in the bonding region in the cold spray is still not well understood. Two questions thus arise: What is the smallest grain size formed in cold sprayed pure aluminum? What is the bonding feature of metal powder particles in the bonding region? In this study, we focus on the microstructure characterization in the particle–particle bonding regions in cold sprayed pure aluminum.

Spherical gas-atomized pure aluminum powder (99.9%) was used as the feed stock. The powder particles were deposited on a grit-blasted Al 7075 alloy substrate by a CGT's Kinetiks 3000 cold spraying system. Nitrogen was used as the process gas to accelerate the powder under a gas temperature and pressure of 523 K and 3.5×10^6 Pa, respectively. The average velocity of the aluminum powder particles was 665 m/s as measured by a time-of-flight optical particle diagnostic system (Tecnar DPV 2000). A field emission scanning electron microscope (FEG-SEM) equipped with an electron backscattered diffraction (EBSD) system was used to characterize the as-received aluminum powder and as-sprayed coatings. Specimens for transmission electron microscopy (TEM) characterization were taken from the as-sprayed aluminum. The TEM characterization was carried out in a Philips CM200 system with a point-to-point resolution of 0.24 nm. Ten specimens were prepared and characterized to search for the particle–particle bonding region and to correlate microstructure evolution and deformation conditions during a short time period of powder particle impact.

Fig. 1(a) and (b) show that the as-received aluminum powder particles are spherical with an average diameter of 36 μm. Larger particles contain multiple equiaxed grains 5–20 μm in size, while the smaller particles are typically single crystals. Fig. 1(c) presents the as-sprayed aluminum particles on the top surface of the coating, implying the severe plastic deformation of particles during the CS process. Fig. 1(d) shows the cross-section of the coating with an average thickness of ~300 μm. The EBSD map of the cross-section of the coating and corresponding grain size distribution are displayed in Fig. 1(e)–(f), showing a very heterogeneous microstructure with a large grain size distribution, ranging from about 9 μm to smaller than 1 μm. Small dots in the EBSD map (Fig. 1(e)) are found in the particle–particle bonding regions, implying those areas cannot be indexed by the EBSD system or the grain size is too small (<100 nm) due to the resolution of the EBSD system.

Fig. 2(a) shows the simulation results of the plastic strain distribution of two impacted particles at 65 ns. We observe gradient strain distribution from the particle center to the particle–particle bonding interface. Fig. 2(b) and (c) show the bright and the dark field TEM images of two bonded aluminum particles. Fig. 2(b) reveals a gradient in grain size from the particle center towards the bonding region. In region *i* (the area about 2 μm from the particle–particle interface), the TEM image (Fig. 2d) shows a microstructure with equiaxial grains about ~200–400 nm in size (Fig. 2(g)) (Details of the grain size measurement are shown in the Supplementary Information). In the region *ii*, the grain sizes are in the nanoscale regime, with an average grain size of ~24 nm ((Fig. 2(e) and (h)). In region *iii* (the particle–particle interfacial region), extremely fine grains are observed, with an average grain size of ~13 nm (Fig. 2(f) and (i)). Of significance is that the frequency of grain sizes below 10 nm reaches about 30%, indicating that the formation of 10-nm grains can be achieved using the CS method. The gradient in grain size along the direction from the particle center towards the particle–particle bonding region could be attributed to the gradients of strain, strain rates and cooling rates, as indicated in the simulation results (Fig. 2 and Supplementary Information).

Fig. 3(a) and (b) show the bright and the dark field images of a region close to the particle–particle interface, respectively, suggesting that the particle–particle interface is completely nanocrystalline. The diffraction pattern in the inset of Fig. 3(a) suggests that the particle–particle bonding region consists of nanocrystalline grains of varying orientations. A high-resolution TEM (HR-TEM) image of the nanoscale grains near the interface (Fig. 3(c)) indicates a high misorientation angle between these nano-sized grains.

The bonding morphology is shown in Fig. 4(a) and (b). Several roll-ups and bulges of approximately 100 nm in size appear on the edges of the particles, indicated by a circle, showing a strongly perturbed morphology (Fig. 4(a)). These roll-ups and bulges are also observed in the particle–particle contact regions, resulting in blurring and mixing of the original particle interface (Fig. 4(b)). It is interesting to find that these features are almost equidistantly distributed and interlocked, forming a zipper-like structure (indicated by arrows in Fig. 4(b)), which could mechanically bond two particles. This morphology suggests that mechanical bonding occurs between the two impacted powder particles in the cold spray process.

The formation of the observed nanoscale grains could be attributed to the extremely high strain, strain rate, and cooling rate in the particle–particle interface. In comparison with the deformation conditions for the 68-nm grains in aluminum observed by Xu et al. [11], the aluminum particles in our study experience similar strain (~10–12) and six orders of magnitude higher strain rate (up to 10^9 s^{-1}) , which are reported in literature [25] and confirmed by our finite element simulation in the Supplementary Information. Here, the high strain rate plays an essential role in the grain refinement. Although the cold sprayed particles may experience a

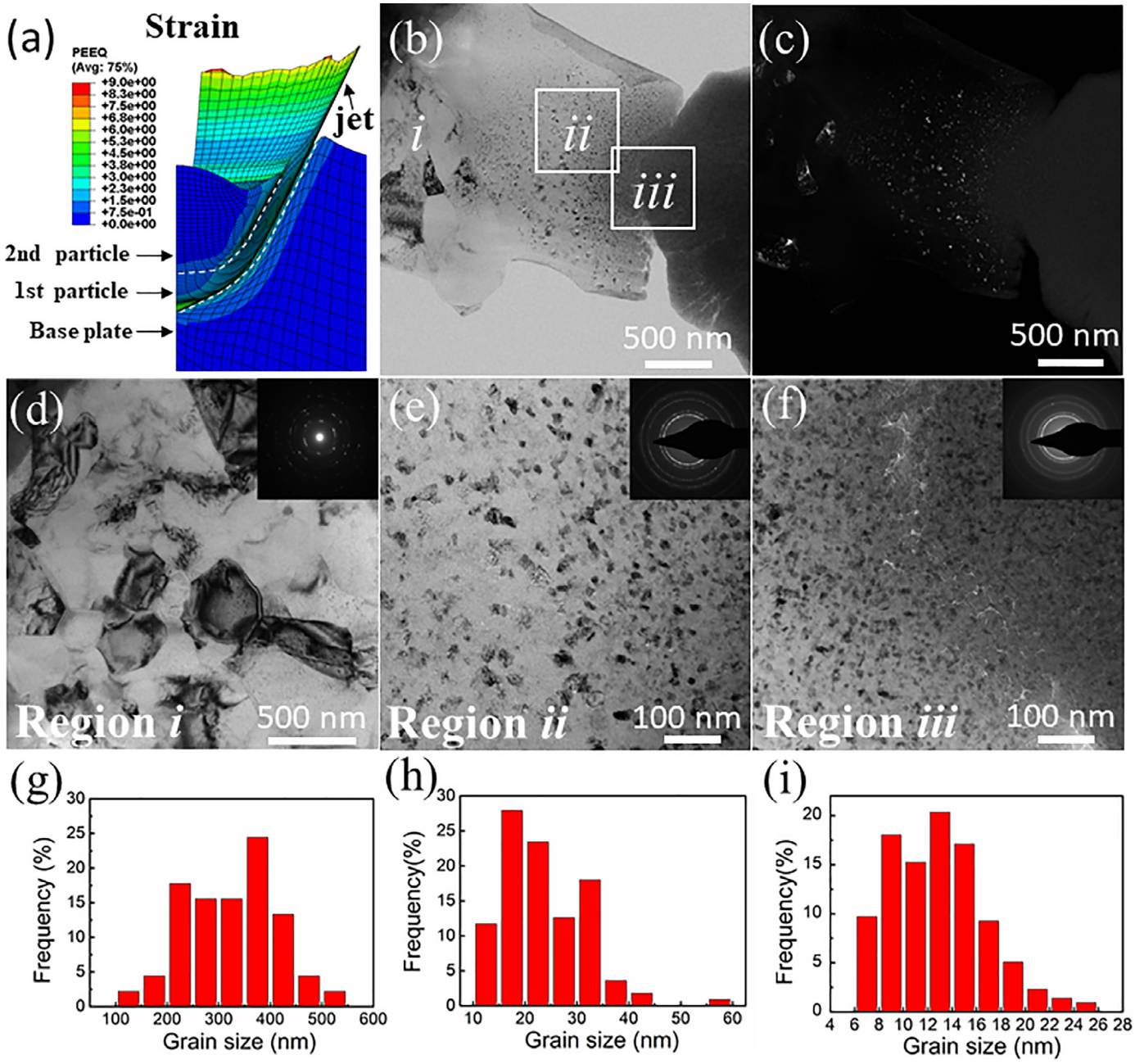

Fig. 2. (a) FEM simulation of the strain distribution of two bonded particles (at 65 ns). Bright field (b) and dark field (c) TEM images of two bonded aluminum particles. Bright field TEM images and statistic grain size distributions for the selected regions in (b): (d) and (g) for region *i* (including an area out of (b)); (e) and (h) for region *ii*; (f) and (i) for region *iii*.

higher temperature than those reported in Xu et al. [11], the local cooling rate is extremely high (up to 10^{10} K/s) [17,25,26], enhancing grain refinement. The microstructure with nanoscale grains in the particle–particle bonding region in this study is very similar to those in the shear banding region of bulk materials under high strain-rate deformations [27]. Meyers et al. [28] and Hines et al. [29] suggested that grains within adiabatic shear bands are refined by rotational dynamic recrystallization. Under the similar high strain and strain-rate conditions in the bonding region, it seems reasonable to use rotational dynamic recrystallization to describe the formation of the nano-sized grains in the cold sprayed aluminum, which is schematically shown in Fig. 3(d). During particle impact, the dislocation density in the previously coarse-grained material increases dramatically. These dislocations accumulate and rearrange into low-angle grain boundaries (LAGBs), forming subgrains. To accommodate the increasing strain, the misorientation angle of the subgrain boundaries increases, the subgrains rotate, and eventually high-angle grain boundaries (HAGBs) and randomly oriented fine grains are formed. To determine the approximate time scale necessary for the formation of the subgrains and HAGBs, the period of time (t) for subgrain rotation is predicted by a kinetic model proposed by Doherty and Szpunar [30]:

$$t = l^2/3\,E_0\,Bb \tag{1}$$

where E_0 is $Gb/4\pi(l-\nu)$ with G the shear modulus (26 GPa), b the Burgers vector (0.286 nm), ν the Poisson's ratio (0.35), and l the subgrain size (~10 nm). B is the dislocation climb mobility by bulk diffusion, calculated by $B = 4dbD/lkT$, where d is about $180b$, k is

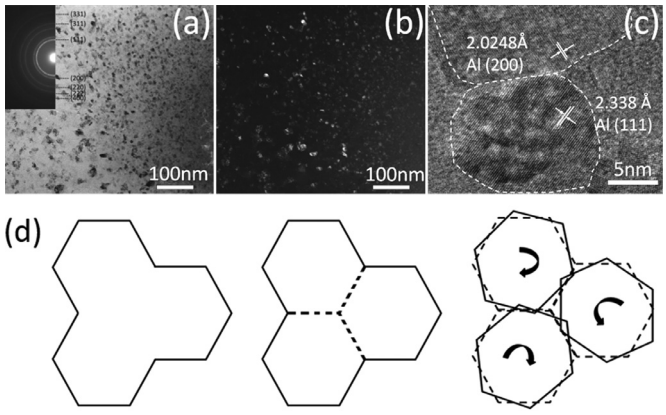

Fig. 3. Bright field image (a) and dark field image (b) of a region close to the particle–particle interface; the inset of (a) shows the corresponding selected area electron diffraction (SAED) pattern; (c) HR-TEM image of nano-grains near the bonding region. (d) Schematic diagram showing dynamic recrystallization produced by subgrain rotation during the particle–particle bonding process.

the Boltzmann constant, T is the temperature in the highly deformed region (~650 K from the FEM simulation) and D is the bulk diffusion coefficient under T (~10–12 m^2 s^{-1}) (values above for aluminum) [30]. Under these conditions, the predicted time of the subgrain rotation is in the range of 150–200 ns, which is similar to the impact time estimated by our FEM simulation (Supplementary Information) and reported in literature [26]. Therefore, the whole process schematically shown in Fig. 3(d) can be achieved during the impact of particles in the cold spray process.

The observed nanoscale interlocking, as marked in Fig. 4(b), is attributed to the high-velocity impact of powder particles. The average velocity of aluminum particles in our experiment is 665 m/s (above the critical particle velocity for adiabatic heating in cold spray of aluminum [19]), so adiabatic heating in the shear bands can cause the materials to soften and deform locally, easily creating shear instabilities and giving rise to viscous flow [21,31]. Under such circumstances the interfacial instability (e.g., roll-ups and bulges in the bonding region) can be explained using the Kelvin–Helmholtz instability phenomenon, as suggested by Grujicic et al. [32]. If there is enough velocity difference across the interface between two particles during the impact, the presence of a defect along the flow path can cause a centrifugal force, which arise in the following particles due to the interface instability. Such force will make materials flow easily, give rise to interfacial roll-ups and bulges, and lead to strongly mechanically interlocked particles. Such bonding mechanism in the cold spray process is fundamentally different from that in cold welding [33], which is mechanically assisted by fast surface-atom diffusion. Furthermore, the phenomena of formation of nano-size grains and nanoscale interlocking in the particle–particle interfacial regions may be correlated. The local high strain and strain rate induce significant grain refinement. Such grain refinement, if the grain size is small enough, might enhance local softening due to the inverse Hall–Petch effect via grain boundary motion [34]. Further studies are needed to confirm how these two effects are coupled.

In summary, we studied the microstructure characteristics and bonding features in the particle–particle bonding region in cold sprayed pure aluminum. We have observed a gradient grain size, from below 10 nm to about 500 nm, near the particle–particle bonding region. The grain size smaller than 10 nm can be achieved in the cold spray process, which has been rarely observed using other deformation methods. The formation of the nanoscale grains can be attributed to the dynamic recrystallization via subgrain rotation at high local strain, strain rate, and cooling rate conditions. Our results suggest that the cold spray method offers a new opportunity to produce nanocrystalline, low melting temperature metals. In addition, nanoscale roll-ups and bulges are formed in the particle–particle interface, leading to strong particle–particle interlocked bonding in the cold spray process. Our observation on the nanoscale interlocking structure provides direct evidence to the bonding mechanism in the cold spray process.

Acknowledgements

This work was developed with the financial support from the Discovery Grants Program (RGPIN-2018-05731) of the Natural Sciences and Engineering Research Council of Canada (NSERC)

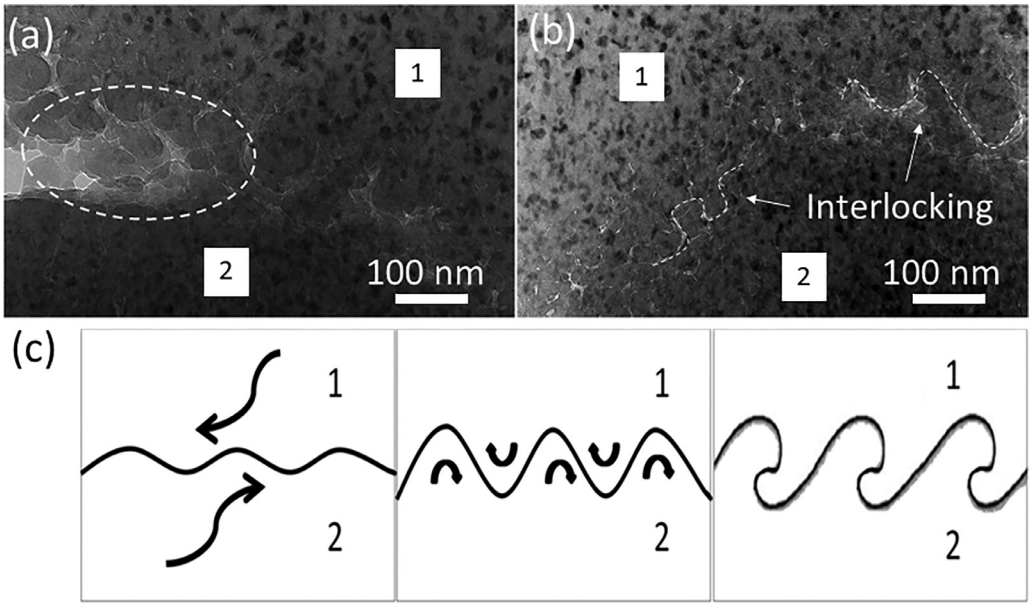

Fig. 4. (a) and (b) show a high magnification of the particle–particle bonding interface. The circle in (a) indicates the morphology of roll-ups and bulges in the bonding region. The arrows in (b) indicate the interfacial perturbations between particle 1 and 2. The arrows indicate the interlocking structure between the two particles. (c) Schematic diagram of the morphology formed due to adiabatic shear instability caused by the particle impact in the cold spray process.

and Dean's Spark Assistant Professorship in the Faculty of Applied Science & Engineering at the University of Toronto. The authors would like to thank Dr. X.D. Liu for his help with the TEM characterization.

Supplementary material

Supplementary material associated with this article can be found, in the online version, at doi:10.1016/j.scriptamat.2019.09.018.

References

[1] L. Lu, M. Sui, K. Lu, Science 287 (5457) (2000) 1463–1466.
[2] T. Chookajorn, H.A. Murdoch, C.A. Schuh, Science 337 (6097) (2012) 951–954.
[3] K. Lu, Nat. Rev. Mater. 1 (5) (2016) 16019.
[4] H. Choi, S. Lee, J. Park, D. Bae, Scr. Mater. 59 (10) (2008) 1123–1126.
[5] C. Xu, Z. Horita, T.G. Langdon, Acta Mater. 55 (1) (2007) 203–212.
[6] J.-.Y. Chang, J.-.S. Yoon, G.-.H. Kim, Scr. Mater. 45 (3) (2001) 347–354.
[7] H. Pirgazi, A. Akbarzadeh, R. Petrov, L. Kestens, Mater. Sci. Eng. 497 (1) (2008) 132–138.
[8] W. Li, N. Tao, K. Lu, Scr. Mater. 59 (5) (2008) 546–549.
[9] K. Wang, N. Tao, G. Liu, J. Lu, K. Lu, Acta Mater. 54 (19) (2006) 5281–5291.
[10] T. Sakai, A. Belyakov, R. Kaibyshev, H. Miura, J.J. Jonas, Prog. Mater. Sci. 60 (2014) 130–207.
[11] W. Xu, X.C. Liu, K. Lu, Acta Mater. 152 (2018) 138–147.
[12] Q. Liu, X. Huang, D. Lloyd, N. Hansen, Acta Mater. 50 (15) (2002) 3789–3802.
[13] M. Chen, E. Ma, K.J. Hemker, H. Sheng, Y. Wang, X. Cheng, Science 300 (5623) (2003) 1275.
[14] V.K. Champagne, The Cold Spray Materials Deposition Process, Elsevier, 2007.
[15] A.C. Hall, L.N. Brewer, T. Roemer, J. Thermal Spray Technol. 17 (3) (2008) 352–359.
[16] H. Assadi, H. Kreye, F. Gärtner, T. Klassen, Acta Mater. 116 (2016) 382–407.
[17] T. Schmidt, F. Gärtner, H. Assadi, H. Kreye, Acta Mater. 54 (3) (2006) 729–742.
[18] L. Ajdelsztajn, J.M. Schoenung, B. Jodoin, G.E. Kim, Metall. Mater. Trans. A 36 (3) (2005) 657–666.
[19] C. Borchers, F. Gärtner, T. Stoltenhoff, H. Kreye, J. Appl. Phys. 96 (8) (2004) 4288–4292.
[20] C. Borchers, F. Gärtner, T. Stoltenhoff, H. Kreye, Acta Mater. 53 (10) (2005) 2991–3000.
[21] H. Assadi, F. Gärtner, T. Stoltenhoff, H. Kreye, Acta Mater. 51 (15) (2003) 4379–4394.
[22] M. Hassani-Gangaraj, D. Veysset, V.K. Champagne, K.A. Nelson, C.A. Schuh, Scr. Mater. 162 (2019) 515–519.
[23] H. Assadi, F. Gärtner, T. Klassen, H. Kreye, Scr. Mater. 162 (2019) 512–514.
[24] M. Hassani-Gangaraj, D. Veysset, V.K. Champagne, K.A. Nelson, C.A. Schuh, Acta Mater. 158 (2018) 430–439.
[25] Y. Xiong, K. Kang, G. Bae, S. Yoon, C. Lee, Appl. Phys. Lett. 92 (19) (2008) 194101.
[26] G. Bae, Y. Xiong, S. Kumar, K. Kang, C. Lee, Acta Mater. 56 (17) (2008) 4858–4868.
[27] A. Mishra, M. Martin, N. Thadhani, B. Kad, E.A. Kenik, M. Meyers, Acta Mater. 56 (12) (2008) 2770–2783.
[28] M.A. Meyers, Y.B. Xu, Q. Xue, M.T. Perez-Prado, T.R. McNelley, Acta Mater. 51 (5) (2003) 1307–1325.
[29] J.A. Hines, K.S. Vecchio, S. Ahzi, Metall. Mater. Trans. A 29 (1) (1998) 191–203.
[30] R.D. Doherty, J.A. Szpunar, Acta Metall. 32 (10) (1984) 1789–1798.
[31] G.B. Olson, J.F. Mescall, M. Azrin, in: Shock Waves and High-Strain-Rate Phenomena in Metals, Springer, 1981, pp. 221–247.
[32] M. Grujicic, J.R. Saylor, D.E. Beasley, W.S. DeRosset, D. Helfritch, Appl. Surf. Sci. 219 (3–4) (2003) 211–227.
[33] Y. Lu, J.Y. Huang, C. Wang, S. Sun, J. Lou, Nat. Nanotechnol. 5 (2010) 218.
[34] M. Legros, D.S. Gianola, K.J. Hemker, Acta Mater. 56 (14) (2008) 3380–3393.